Submicrosecond scan-angle switching photonic beamformer with flat RF response in the C and X Bands

Submicrosecond Scan-Angle Switching Photonic Beamformer With Flat RF Response in the C and X Bands

Oded Raz, *Member, IEEE*, Sharon Barzilay, Ruth Rotman, and Moshe Tur, *Fellow, IEEE, Fellow, OSA*

***Abstract*—A wideband (>10 GHz) beamformer, based on a photonic true-time-delay, with submicrosecond scan-angle switching is reported. The smooth microwave transmission (ripples <0.5 dB and $<3°$) and superb uniformity among the elements (<0.1 dB and $<0.5°$) are then used for the processing of 1 GHz-wide linear frequency modulation (LFM) signals in both the C and X bands with excellent performance. This performance is also maintained under dynamic operation, where a fast tunable laser is employed to provide <300 ns wavelength-controlled angle scanning. Based on these characteristics, an optimized architecture, where a photonic beamformer feeds a series of classical subarrays, can offer high performance in both the time and spatial domains for large, wideband phased-array antennas, with wide scan angles.**

***Index Terms*—Array signal processing, microwave photonics, optical antenna beamforming, optical signal processing, radar.**

I. Introduction

PHOTONIC implementations of RF true time delay (TTD) [1] should prove beneficial for next generation wide bandwidth radar systems [2]. A photonic beamformer can have an almost distortion-less, very wideband RF transfer function between the array input port (in transmit) and each of the output ports, which feed the antenna elements. Moreover, in order for the multielement beamformer to generate a clean spatial beam and a sharp temporal impulse response [when the input RF pulse is phase coded, e.g., in the case of linear frequency modulation (LFM)] [2], very high degree of uniformity is required among the transfer functions of the different elements. Finally, fast angle switching (of the order of microseconds) is desired for the successful operation of advanced reconfigurable radars, where pulses transmitted along various lines of sight and/or modes need to be interleaved within a few microseconds [5], [6].

Previously demonstrated photonic beamformers, e.g., [7]–[], have concentrated on the time delay performance of the suggested designs. However, the need to maintain smooth microwave performance of each TTD element over a very wide bandwidth, and even more importantly: the necessity to maintain uniform performance among all TTD devices used in the same array, was only partially addressed.

Previously, [13], we have described a wavelength-controlled photonic TTD module, having excellent RF characteristics. Based on this building block, and using a fast tunable laser for angle steering [14], we present in this paper measured results for a four channel photonic beamformer (Section II), with very smooth RF response in both the C and X bands, and minute variations among the RF transfer functions of the four TTD channels (Section III). The beamformer is then tested for transmission of a 1–GHz LFM signal, while the tunable laser is being switched between different wavelengths, Section IV. Finally, the performance of the photonic beamformer as a building block for a large phased array, having a series of subarrays, employing classical phase shifters is discussed, Section V, followed by concluding remarks.

II. Beamformer Design

The four channel beamformer is shown in Fig. 1.

Light coming from the fast tunable laser was double-sideband modulated by the RF source, using an in-quadrature biased Mach-Zehnder $LiNbO_3$, electrical to optical (E/O) converter. The modulated light was then amplified and evenly split among the four channels. While Channel 1 served as a reference, comprising only a length of fiber, the other three channels included a passive photonic TTD (PTTD), mentioned in [12] and described in detail in [13]. An eight port, thin film optical demultiplexer (DeMux) was used to accomplish the wavelength-controlled TTD operation, as shown in the inset in Fig. 1. The input modulated light is sent through a circulator into the DeMux, where, depending on its wavelength, it is routed to a particular output port. A different length of fiber (having a highly reflective $(\sim 100\%)$ silver coated tip) is spliced to each output port of the DeMux, with a predetermined increment from port to port. Thus, the returned light emerging from the circulator into the photodetector (O/E) experienced a wavelength–controlled pure delay, which is practically dispersion-free. Extremely fast angle switching is achieved here using a commercial fast tunable semiconductor laser [16], [17], with a rated switching time of 200 ns (between any two wavelengths on a 50-GHz grid, covering the wavelength range of 1530–1560 nm), maximum output power of $+9$ dBm, and a measured RIN of less than -150 dB/Hz. For proper pulsed operation of the beamformer, the RF source and the tunable laser must be time synchronized, see later

Manuscript received January 31, 2008; revised May 29, 2008. Current version published October 10, 2008.

O. Raz is with the School of Electrical Engineering, Tel-Aviv University, Tel-Aviv, Israel. He is also with Eindhoven's University of Technology, Eindhoven, The Netherlands (e-mail: o.raz@tue.nl).

S. Barzilay, R. Rotman, and M. Tur are with the Interdisciplinary Studies, School of Electrical Engineering, Tel Aviv University, Ramat Aviv, Tel Aviv, Isael, (e-mail: Sharon.barzilay@gmail.com; rotman@eng.tau.ac.il; tur@eng.tau.ac.il).

Color versions of one or more of the figures in this paper are available online at http://ieeexplore.ieee.org.

Digital Object Identifier 10.1109/JLT.2008.927150

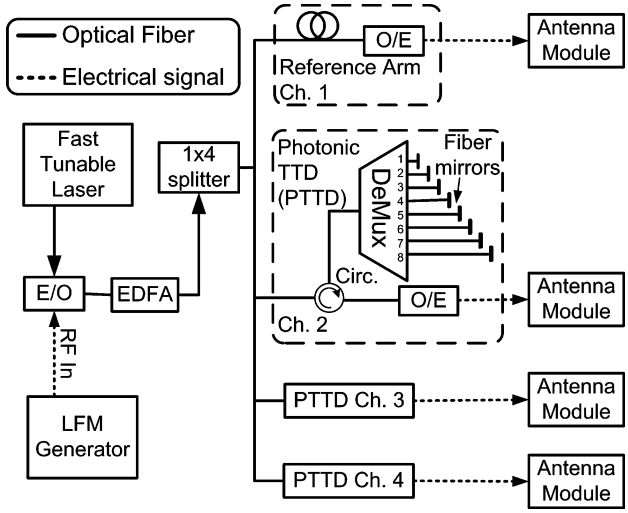

Fig. 1. Schematic drawing for a four-channel PTTD beamformer. The output of each TTD module can either feed an antenna element or a subarray of a few antenna elements, see Section V [15].

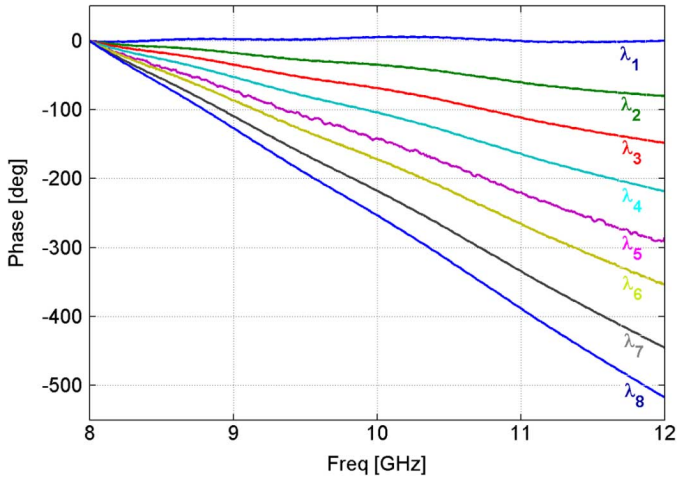

Fig. 2. The RF phases for eight wavelengths $(\lambda_1, \ldots, \lambda_8)$ going through Channel 3 of the beamformer, having a designed incremental delay change of 50 ps between consecutive wavelengths (λ_1 is used a reference).

Fig. 8. The high output power of the laser and the EDFA optical gain compensate for the insertion loss of the Mach-Zehnder Modulator (E/O), the photonic TTD (about 5 and 7 dB, respectively), as well as the 7–dB insertion loss of the splitter. It is also of importance to bring the optical signal at the input of the O/E to the maximum unsaturated power tolerated by the photodetector ($>$ 10 dBm), thereby minimizing thermal noise contributions [13], [18]. The photodetectors were chosen to have closely matched RF response to ensure uniformity among the four TTD channels. All channels (excluding channel 1) have the same type of DeMux but different lengths of fiber are spliced to the ports of the channel DeMux. If the length *increment* between neighboring ports of the DeMux of Channel 2 is ΔL, then in order to achieve linear angle scanning the corresponding length increments of channels 3 and 4 should be $2\Delta L$ and $3\Delta L$, respectively. If one adjusts port 1 of all TTDs to provide the same delay as the reference fiber of channel 1, then by tuning the laser to that wavelength, which goes through port 1, one achieves a *forward* propagating transmitted wavefront. Tuning the laser to a different wavelength will result in a tilted wavefront. Bidirectional scanning can also be accomplished by simple addition of delay lines (see Section V).

III. The CW RF Performance of the Beamformer

An RF vector network analyzer (VNA) was used to characterize the RF transfer function of the four TTD channels, with its RF output replacing the RF source in Fig. 1, and its input connected to the output of the O/E module of the channel under study. For these measurements the fast tunable laser was set to work as a tunable CW source, and for each of the four channels, the magnitude and phase of the forward transmission coefficient $S_{21}(f)$ were recorded for all eight wavelengths supported.

A. Delay Characteristics

Fig. 2 plots the (unwrapped) RF phase $(\angle S_{21}(f))$ as a function of the RF frequency for Channel 3 at the 8 operating wavelengths, using $\lambda_1 (= 1547.72$ nm) and Channel 1 as the zero delay reference.

TABLE I
Measured Delays of Beamformer [ps]

Wavelength [nm]	Ch. 1	Ch. 2	Ch. 3	Ch. 4
λ_1=1547.72	0	0	0	0
λ_2=1549.32	0	49	102	150
λ_3=1550.92	0	112	200	301
λ_4=1552.52	0	156	294	451
λ_5=1554.13	0	203	399	601
λ_6=1555.75	0	250	493	745
λ_7=1557.36	0	296	595	898
λ_8=1558.98	0	351	697	1052

The measured delays, given by the scaled derivative $(1/2\pi)d(\angle S_{21}(f))/df$ (with $\angle S_{21}(f)$ in radians and f is in Hz), are shown in Table I for all four channels, exhibiting increments of 50 ps for Channel 2, 100–ps increments for Channel 3, and 150–ps increments for Channel 4, with a mean absolute deviation of 3 ps and an RMS value of less than 4.3 ps. Note that the delays for the reference wavelength $\lambda_1 = 1547.72$ nm were set to zero also for Channels 2–4, since one can always add line stretchers at the receivers outputs to achieve the required alignment for an arbitrary number of channels.

Careful examination of the curves of Fig. 2 reveals, however, that they slightly deviate from straight lines, exhibiting small phase ripples. In the next subsection, the magnitude and phase ripples of $S_{21}(f)$ are presented and shown to be very small over large RF bandwidths, thereby promising high quality microwave transmission of wideband ripple-sensitive signals (e.g., LFM [19]).

B. RF Transfer Characteristics

Full RF characterization of the photonic beamformer involves the evaluation of 32 RF links, comprising four channels with eight wavelengths per channel. Before presenting the results

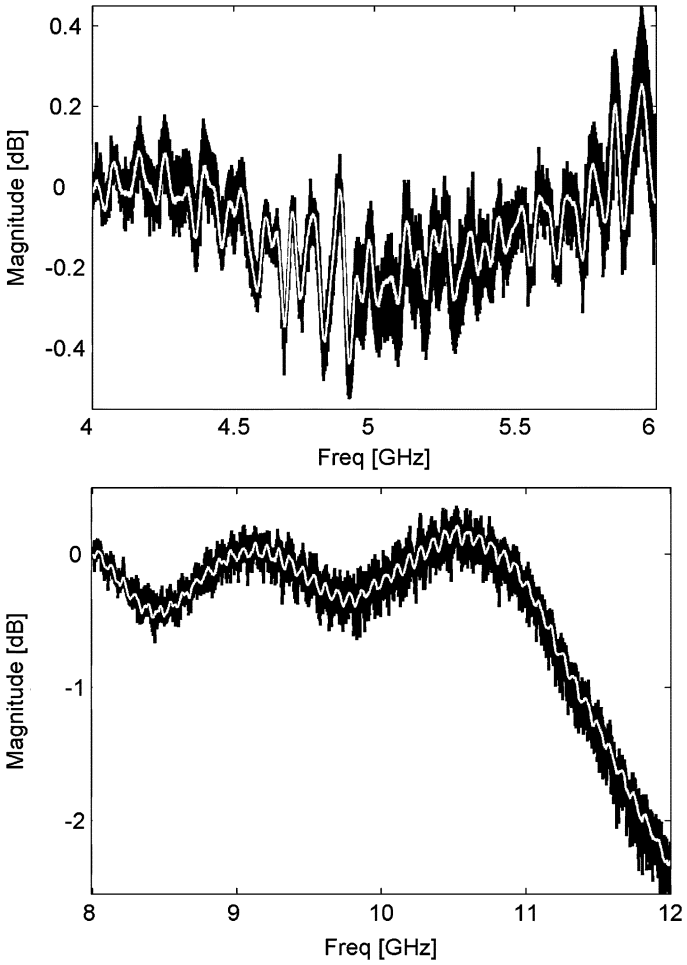

Fig. 3. The measured frequency dependence of the magnitude of S_{21} (after its frequency-averaged value has been subtracted) for all four channels at all eight wavelengths, resulting in 32 superimposed curves. The white line is the per-frequency mean, and most of the C and X microwave bands is covered.

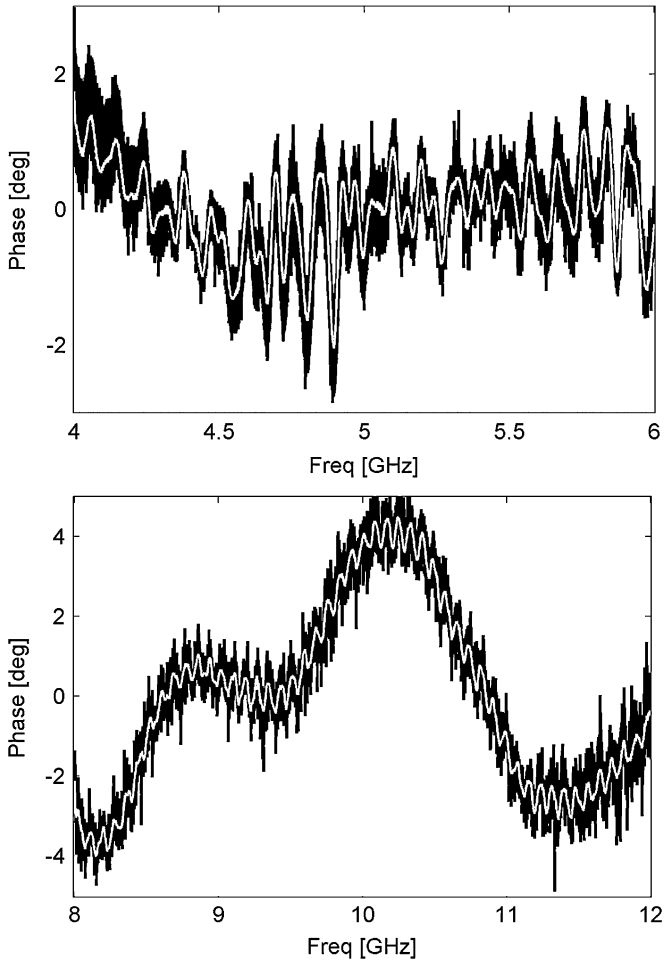

Fig. 4. The measured deviations of the RF phase from a linear dependence on frequency. The results for the 32 RF links are superimposed to show the small deviations from the mean (heavy line).

for the magnitude of $S_{21}(f)$, we note that the *frequency-averaged* per-link RF insertion loss, $\langle 20\log_{10}|S_{21}(f)|\rangle_f$, did vary among the measured 32 links due to varying amount of optical loss among the $25(=3X8+1)$ different optical routes involved. Thus, Fig. 3 shows, *superimposed*, the per-link frequency dependence of the magnitude of S_{21} for each of the 32 RF links, but only after its frequency-averaged value, has been subtracted (i.e., $|S_{21}(f)|_{\rm dB} - \langle |S_{21}(f)|_{\rm dB}\rangle_f$, where $|S_{21}(f)|_{\rm dB} = 20\log_{10}(|S_{21}(f)|)$), resulting in 32 superimposed curves. While the white line represents the per-frequency mean value, averaged over the 32 measured RF links (including the reference channel), the black area portrays the nonzero, though very small deviations from that mean. Fig. 4 studies the deviations of the phase versus frequency curves of Fig. 2 from straight lines (together with similar curves for the other three channels).

Table II summarizes the statistics of the deviations of $|S_{21}(f)|_{\rm dB}$ and $\angle S_{21}(f)$ from straight lines, indicating high degree of flatness over quite a wide RF spectrum.

All wavelengths exhibit virtually the same RF performance. For example, the measured deviations of the RF magnitude and phase response of $\lambda_2,\ldots,\lambda_8$ from those of λ_1 for Channel 2

TABLE II
STATISTICS (OVER FREQUENCY) OF THE MAGNITUDE AND PHASE RESPONSES

Band	Maximum Variations of the Magnitude [dB]	Standard Deviation of the Magnitude [dB]	Maximum Variations of the Phase [deg]	Standard Deviation of the Phase [deg]
4-6GHz	±0.4	0.077	±3	0.467
8-12GHz	±0.3*	0.110*	±4	0.444

* These variations are within the passband of the modulator, not including the sharp drop above 11GHz

were found to be smaller than 0.05 dB and 0.2°, respectively. Fig. 5 shows that in spite of the fact that the four channels were equipped with *different* (though of the same brand) demultiplexers, O/E converters and associated circuitry, both the magnitude and phase responses are practically independent of the channel tested. This high degree of inter-channel uniformity among the 32 RF links leads us to 'blame' their only common component, namely: the E/O converter, for the ripples in the white line representing the mean value in Figs. 3 and 4. These larger frequency-dependent ripples may be characterized by two frequency scales: The slow variations with respect to the RF frequency are attributed to the (off-the-shelf) integrated-optics modulator itself (most notably is the cutoff at ~11 GHz),

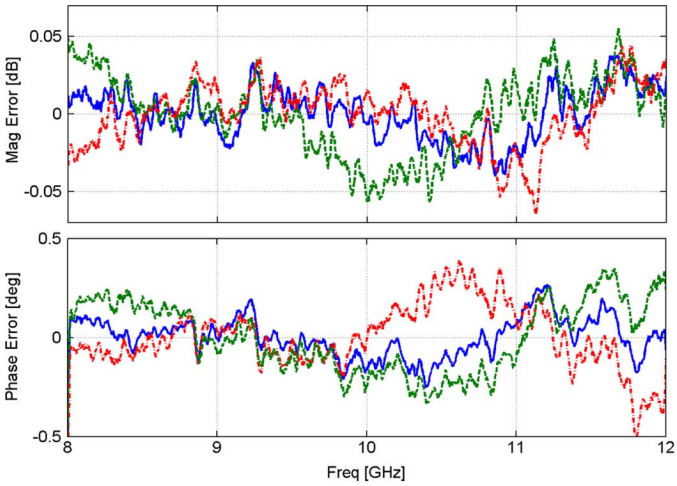

Fig. 5. The (measured) deviations of the RF magnitude and phase of Channels 2, 3, and 4 from those of Channel 1 at λ_1.

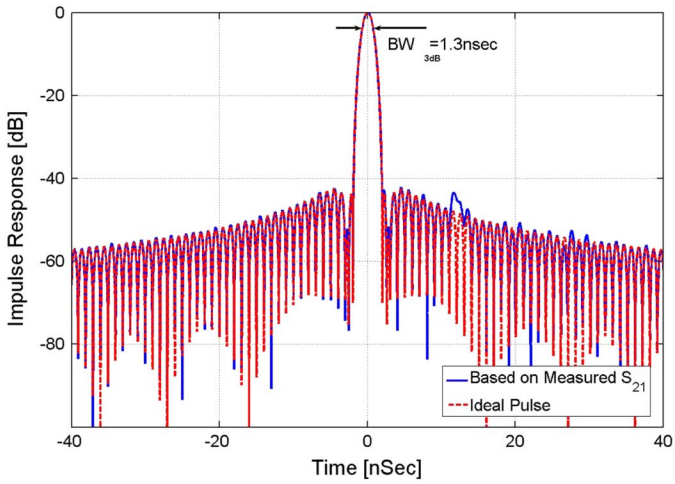

Fig. 6. The impulse response of a processed 1–GHz LFM pulse, using an apodizing Hamming window. The dotted line represents the ideal case of undistorted pulse, while the solid line is simulated impulse response of an ideal LFM pulse when distorted by the transfer function, taken from the white line of Figs. 3 and 4 (i.e., $H_{\text{system}}(f) = \langle S_{21}(f) \rangle$).

whereas the fast sinusoidal variations probably originated from the modulator driving circuitry and parasitic reflections. The deleterious effect of frequency domain fluctuations on the transmission of wideband LFM pulses is dicussed in detail in [19].

However, the very similar behavior of all RF links in the beamformer of Fig. 1 makes it possible to calibrate out and "flatten" the common ripples, represented by the white lines in Figs. 3–4, thereby achieving yet better RF performance, see Section IV.

In summary, the achieved high quality wideband CW RF transfer characteristics should ensure almost distortion-less pulse transmission, but only if the fast tunable laser does not introduce distortions of its own.

IV. LFM Pulse Transmission Under Angle Switching

Radar systems employ various pulse compression techniques to improve temporal resolution without the need to

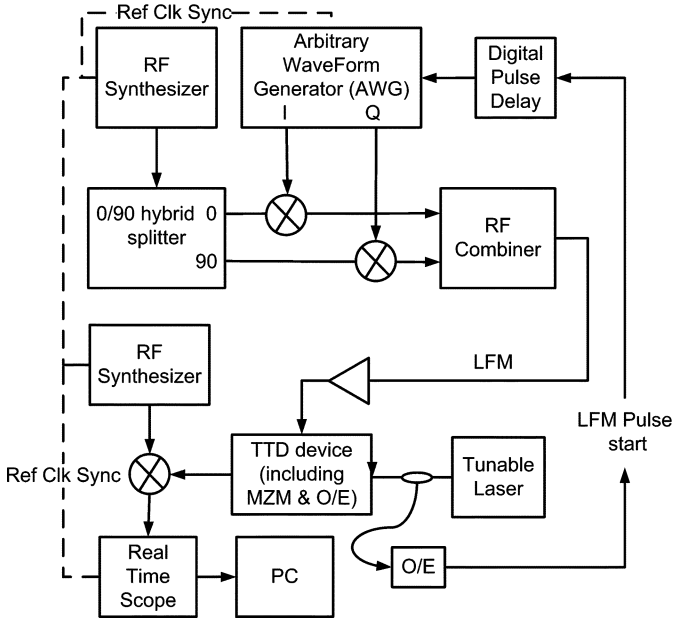

Fig. 7. Experimental setup for the measurement of wavelength fluctuations due to fast switching.

employ impractically high peak power short pulses [2], [5]. A quite common pulse compression technique involves linear frequency modulated (LFM) pulse, numerically defined by [2]

$$V_{\text{in}}(t) = \cos\left[2\pi f_0 t + (\pi B/T)\, t^2\right] \text{rect}[t/T] \tag{1}$$

where f_0 is RF frequency at the center of the pulse, B is the total bandwidth of the signal, and T is the pulse length. During the pulse life ($-T/2 \le t \le T/2$), the instantaneous frequency $f(t) = f_0 + (B/T) \cdot t$, linearly scans the frequency range: $f_0 - B/2 \le f \le f_0 + B/2$. There is, thus a mapping [20] between the instantaneous frequency and time in the pulse, so that when the LFM pulse goes through a nonlinear device it will produce out-of-range-harmonics but not intermodulations, which limit s/n and dynamic range. Upon reception, the LFM signal is correlated with the undistorted original pulse shape, either via weighted matched-filter or dechirp processing [21]. The resulting narrow temporal pulse, the so-called impulse response ($\text{IR}(t)$), shown in Fig. 6, has a width, which is inversely proportional to the bandwidth, B, and sidelobes, whose peak level is ideally determined by the apodizing weighting filter (e.g., Hamming window or equivalent).

For the case of weighted matched filter processing, $\text{IR}(t)$ is given by

$$\text{IR}(t) \propto \Im^{-1}[W(f) \cdot H_{\text{compress}}(f) \cdot H_{\text{system}}(f) \cdot \Im_{\text{LFM}}(f)] \tag{2}$$

where $\Im_{\text{LFM}}(f)$ is the Fourier transform of the LFM signal of (1), $H_{\text{system}}(f)$ represents the transfer function of the system from transmission to reception (ideally, $H_{\text{system}}(f) \propto \exp[-j2\pi f t_d]$ for a pure delay of time t_d), $H_{\text{compress}}(f)$ is the filter used for compression (e.g., the complex conjugate of $\Im_{\text{LFM}}(f)$, for the ideal case when $H_{\text{system}}(f)$ represents a pure delay), and $W(f)$ is a weighting function, e.g., a Hamming window.

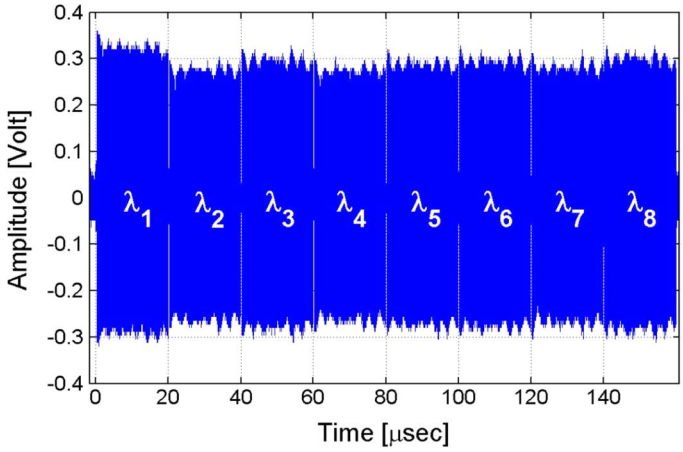

Fig. 8. Measured time series of eight consecutive LFM pulses (X band data, Channel 2).

To succeed as a beamformer, the beamformer of Fig. 1 must not seriously affect the three most important figures of merit of the impulse response of an LFM pulse: (i) the width of the main lobe, which can be broadened by slow ripples in $S_{21}(f)$, (ii) the peak sidelobe level (PSL), which can decrease in case of fast ripples in $S_{21}(f)$; and finally, (iii) the Integrated SideLobe Ratio, defined here for the Hamming apodizing window by [$s(t)$ is the impulse response, T is the length of the LFM original pulse, and $\sigma_{3\text{ dB}}$ is the width of the impulse response at its full width, half maximum (FWHM)]:

$$\text{ISLR[dB]} = 10\log_{10}\left[\frac{\int_{-3\sigma_{3\text{ dB}}}^{3\sigma_{3\text{ dB}}} s^2(t)dt}{\int_{-T/2}^{-3\sigma_{3\text{ dB}}} s^2(t)dt + \int_{3\sigma_{3\text{ dB}}}^{T/2} s^2(t)dt}\right]. \tag{3}$$

Ideally, for a Hamming window, the FWHM of the impulse response is $\sigma_{3\text{ dB}} = 1.3/B$, the PSL is 42 dB below the peak of the main lobe and the ISLR is 34 dB. The solid curve in Fig. 6 describes the simulated effect of the nonideal transfer function of our beamformer on $\text{IR}(t)$: As expected, the effect is very small.

We have previously shown [13] that a microwave photonic channel of the design of Fig. 1 can support high quality 600-MHz-wide LFM transmission. In this paper, we extend those measurements to the practical fast tunable multichannel beamformer of Fig. 1, showing excellent 1 GHz-wide pulse transmission in a submicrosecond dynamic angle scanning environment, as well as superb uniformity among different channels.

Fig. 7 shows the experimental setup used to transmit 1 GHz LFM pulses through the photonic true time delay beamformer under dynamic switching of the tunable laser (namely, the optical carrier is switched in < 300 ns to a different wavelength for every consecutive pulse). An arbitrary wave generator (AWG) with a sampling rate of 1.25 Gb/s generated the required baseband I & Q components of a ± 500 MHz LFM signal with a duration of 20 μs ($B \cdot T = 20\,000$). An RF synthesizer generated the RF carrier at either 5 GHz (C band) or 10 GHz (X band), which was then split in two by a $0^\circ/90^\circ$ hybrid splitter. The I component was mixed with the RF carrier, while the Q was mixed with a 90° phase-shifted version of the same carrier. The sum of these two upconverted signals is the desired LFM signal of (1) with $f_0 = 5$ or 10 GHz, $T = 20$ and $B = 1$ GHz. All parameters of this RF upconversion circuitry (I, Q amplitudes and delays, carrier phases at the LO input of the mixers, etc.) were carefully adjusted to result in > 40 dB rejection of carrier leakage and images. The obtained LFM signal, after some RF amplification, was then used to modulate the laser light. Beam scanning was achieved by programming the required wavelength sequence into the memory of the driving electronics of the tunable laser. In our experiment, the laser switched, consecutively, from λ_1 to λ_2 and so forth up to λ_8, every 20.3 μs, allowing 300 ns for the actual switching and spending 20 μs on the transmission of the LFM pulse at the chosen wavelength. Since the laser output was blanked during a wavelength change, a triggering event for the generation of the LFM pulse could be obtained from the rising optical power, following the blanking period. The exact time gap between the change of optical wavelength and the start of the LFM pulse was carefully controlled by a high resolution digital delay generator.

The modulated laser light simultaneously traveled through the four channels, navigating the routes corresponding to its wavelength, and then converted back to four RF signals, ready to be fed to the antenna elements/subarrays, see Fig. 10. Instead, these four outputs were individually down converted from the C or X bands to occupy the frequency range of 0.5–1.5 GHz, where they were captured by an eight-bit, 4–GHz, 20–Gs/s real time oscilloscope. A typical sequence of eight pulses at the output of Channel 2 is shown in Fig. 8. The digitized pulses were then ready to be processed by a compression filter and a Hamming apodizing window to produce the impulse response.

As shown by the solid line of Fig. 7, the transfer function of the beamformer should not distort the impulse response by much (for a detailed study, see [19]). It turned out, however, that our up- and downconversion circuitry added distortions, which had nothing to do with the quality of the beamformer. To recover high quality impulse responses, we calibrate the system by processing all pulses coming out of the beamformer with a *modified* filter, derived from a reference pulse, recorded *once* at the output of Channel 1, at λ_1. Denoting this reference waveform by $s_{\text{ref}}(t)$, we find

$$\text{IR}(t) \propto \Im^{-1}[W(f) \cdot [\Im_{s_{\text{ref}}(t)}(f)]^{-1} \cdot H_{\text{system}}(f) \cdot \Im_{\text{LFM}}(f)]. \tag{4}$$

Using this reference pulse for decompression, we obtain Fig. 9. It is clearly demonstrated that the impulse response maintains its high quality regardless of the photonic path used.

As explained in (3), the ISLR of the processed LFM signal is an important figure of merit, related to the signal-to-noise ratio (SNR) of the link. Table III summarizes the performance of the photonic beamformer, based on the measured values for the PSL and ISLR.

The achieved ISLR was around 26.5 dB is only 8 dB worse than the ideal value for the apodizing window used. This limited performance was probably due to the limited available microwave power at the modulator input. It also appears that transients accompanying the switching of the tunable laser did not

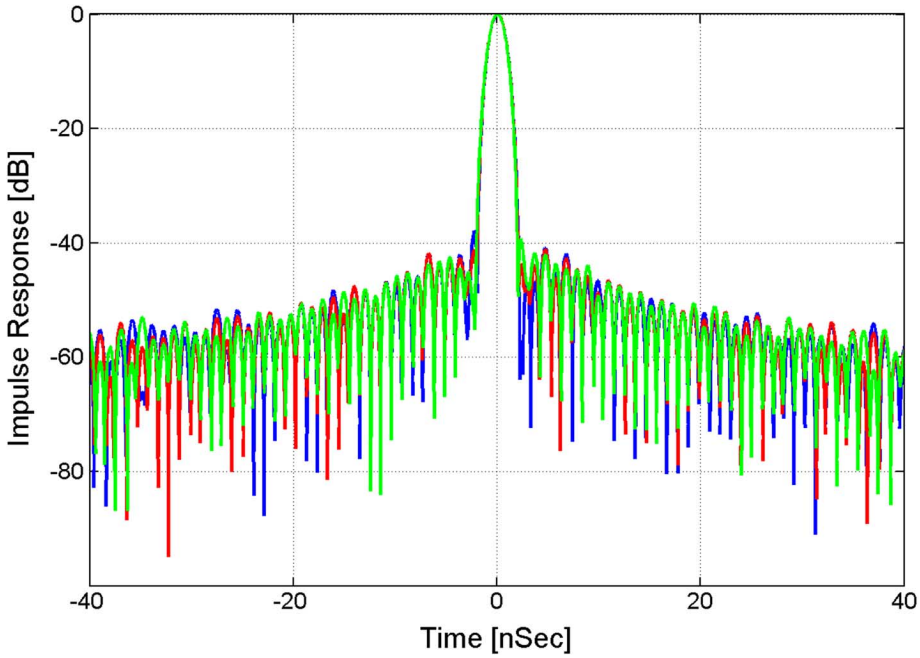

Fig. 9. The impulse response of various photonic paths, processed against a fixed reference taken from Channel 1, λ_1.

TABLE III
FIGURES OF MERIT (FOM) FOR THE IMPULSE RESPONSE OF THE BEAMFORMER

FOM \ Band	C	X
PSL	-39	-39
ISLR	-26.5	-26.5

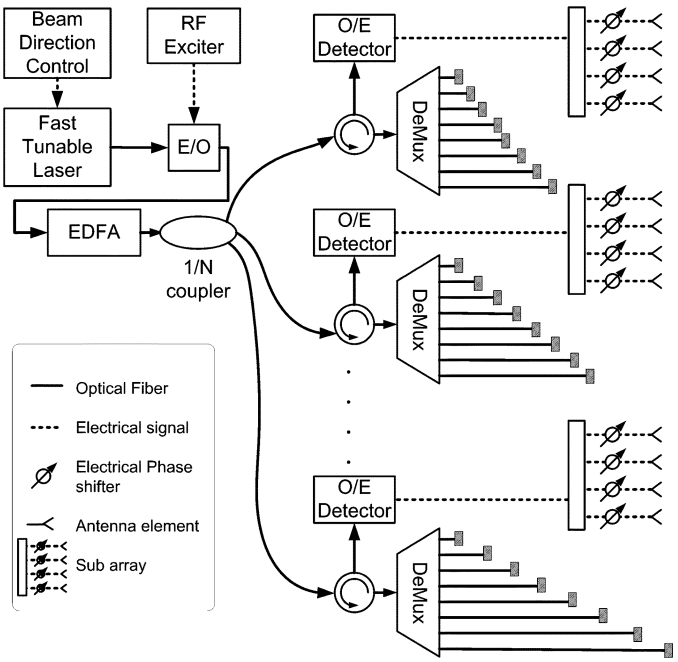

Fig. 10. Schematic drawing of a beamformer comprising N photonic TTD modules, each feeding a four element subarray.

contribute any penalty, since the obtained performance was the same for both CW and switched operation.

V. THE PHOTONIC BEAMFORMER AS A BUILDING BLOCK FOR LARGE PHASED ARRAYS

True time delay beamformers are of particular importance in large, wideband phased array antennas, having wide scan angles. Ultimately, superb performance can be achieved by using the PTTD building block of Fig. 1 to feed each and every antenna element of a large array. The uniformity of the transfer functions between the PTTDs ensures that with calibration via the phase shifters, excellent spatial performance can be achieved, as discussed in detail in [21].

But instead of feeding each antenna element with a PTTD, subarrays may be used, as shown in Fig. 10, at the expense of some quantization errors [15]. Each subarray, inherently small in size, may be of classical design, employing phase shifters. This series of subarrays will be fed, however, by a photonic beamformer of the architecture shown in Fig. 1. The inclusion of phase shifters also allows for overall calibration of the array, compensating for small delay errors in the PTTDs. In view of the excellent uniformity of S_{21} over wavelengths, that is, over beam angles, calibration at a single wavelength appears sufficient. Note that a single control line, at the input of the laser tuning circuitry governs the angle scanning of the complete photonic beamformer. Moreover, a significant percentage of hardware can be remoted from the antenna itself, offering obvious advantages in difficult packaging situations.

The antenna pattern was simulated for an array comprising $Q(=32)$ PTTDs of the design and characteristics of those described in Sections II–III, each feeding a subarray of $P(=4)$ phase shifters for a total of 128 radiating elements, operating in the X band and spatially spaced by a half-wavelength ($d = 0.015$ m@10 GHz). The basic delay of the nth PTTD is $n \cdot 50$ pS, $n = 1 \ldots 32$. Symmetric and bidirectional angle scanning can be achieved by connecting the PTTDs to their corresponding subarrays with cables (e.g., an optical cable between the circulator and the E/O, or an electrical

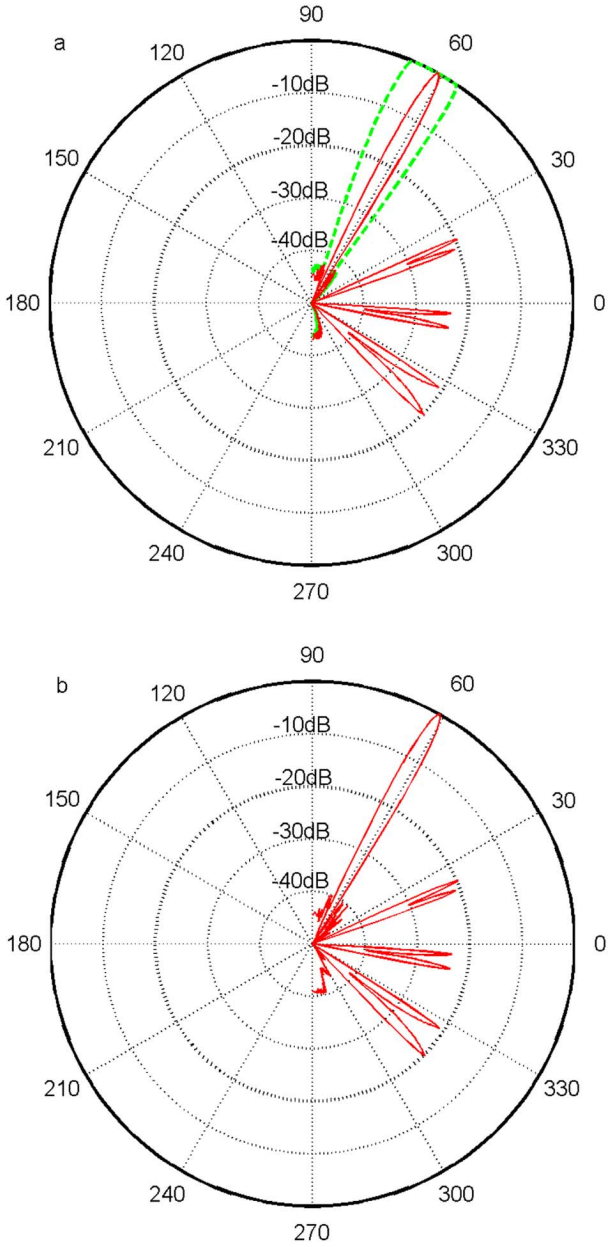

Fig. 11. Antenna patterns for a simulated antenna of 32 PTTDs, each feeding a subarray of four phase shifters. (a) Solid line: the envelope of radiation patterns of an error-free 32×4 array, aimed at 61°, as the carrier frequency covers 1 GHz around 10 GHz. The dashed line is the corresponding curve for an array comprising 128 phase shifters. (b) Same as (a) but including errors in the time delays of the PTTDs, as well as nonuniformities among the 32 PTTDs, see text.

cable between the E/O and the antenna element) of *unequal* lengths, providing unequal wavelength-independent delays $\tau(n), n = 1, \ldots Q$ for the different subarrays. Thus, if these delays obey $\tau(n) - \tau(n+1) = 175$ pS$, n = 1, \ldots (Q-1)$, sequential transmission at λ_1 to λ_8 (at λ_1 all PTTD provide the same delay) will result in the following range of scan angles $[-61^0\ -39^0\ -22^0\ -7^0\ 7^0\ 22^0\ 39^0\ 61^0]$, derived from $\arcsin((n \cdot 50\ \text{pS} - 175\ \text{pS}) \cdot c/(4d))), l = 0 \ldots 7$. At these scan angles, diffraction limited patterns can be achieved at the center frequency $f_0 = 10$ GHz by adjusting the phase shifters not only to tune the subarrays to the right scan angle but also to compensate for inaccuracies in the time delays of the PTTDs (see Table I). However, as the carrier frequency scans a bandwidth of 1 GHz around f_0, the phase shifters give rise to parasitic lobes, whose strength increases as the number of PTTDs decreases.

Fig. 10(a) describes the radiation pattern of the array at the extreme angle of 61°, assuming Hamming weighting of the 128 elements and taking the maximum radiation intensity at each angle as the carrier frequency scans the range of 9.5–10.5 GHz. It is further assumed that all delay lengths are perfect multiples of 50 pS and that all 32 PTTDs share the same RF transmission characteristics over the 9.5–10.5 GHz frequency range. The plot clearly shows a narrow diffraction-limited main lobe, accompanied by unwanted, though -20 dB weaker, quantization lobes [15]. Had we assumed the array to comprise 128 PTTDs, the same main lobe would have resulted but without quantization lobes. The dashed line is the radiation pattern for an array comprising 128 phase shifters. While such an array produces a diffraction-limited beam in the broadside (0°) direction, its wideband (1 GHz) performance at 61° is quite poor, producing a beam much wider than that obtained from the photonic beamformer, albeit without the quantization errors.

In Fig. 10(b), two kinds of errors have been added: i) it is assumed, following Table I, that the built-in delays of the PTTDs have an additive random error of $\sim$5 pS rms (as mentioned earlier this error can be compensated for only at the center frequency f_0, by proper adjustment of the phase shifters); and ii) there exists nonuniformity among the $S_{21}(f)'s$ of the 32 PTTDS, as indicated in Fig. 5. This effect has been taken into account by ignoring the magnitude nonuniformity and by assuming a random phase error among the PTTDs over the relevant frequency range of 0.5° rms. The results show very little degradation.

VI. Conclusion

We have constructed, and successfully demonstrated the operation of a fast switching, four channel photonic ultrawideband true time delay beamformer. The fast 300–ns switching time may prove useful for future phased array architectures. The observed low ripples in magnitude and phase of the beamformer elements over a very large frequency range ($\sim$ 4–12 GHz) enable high-quality transmission of $>$ 1 GHz LFM pulses with very low sidelobe levels. Even better results could have been obtained had the O/E had a flatter RF response. The variations among the microwave responses of the four different elements are minute and substantially better than what can be currently obtained from a similar microwave TTD implementation, where uniformity among channels of less than a few dB's and several degrees are very difficult to achieve [22]. A parallel architecture for receive is now being investigated. With proper use of optical amplification, the architecture can be extended to tens of elements, and to hundreds, when subarrays are employed, enabling true time delay beamforming for ultrawideband phased arrays. For this investigation, apart from the tunable laser (which can be replaced by a bank of lasers, each emitting a different wavelength), all components involved are off-the-shelf, relatively inexpensive items, which are mass-produced for the optical communication industry. Thus, it appears that the proposed photonic beamforming architecture should be, at present, an ad-

vantageous candidate for inclusion in high performance, large phased array applications where TTD is needed. With the advent of silicon-based chip-scale photonic technology, future integrated antennas can make use of compact and cheap versions of this design.

REFERENCES

[1] H. Zmuda and E. N. Toughlian, *Photonic Aspects of Modern Radar*. Boston, MA: Artech House, 1994.

[2] R. J. Mailloux, *Phased Array Antenna Handbook*. Boston, MA: Artech House, 2005.

[3] R. J. Mailloux, "Technology for array control," in *Proc. IEEE Int. Symp. Phased Array Syst. Technol.*, Boston, MA, 2003, pp. 35–39.

[4] J. R. Klauder *et al.*, "The theory and design of chirp radars," *Bell Syst. Tech. J.*, no. 39, pp. 745–808, 1960.

[5] G. W. Stimson, *Introduction to Airborne Radar*, 2nd ed. New York: Scitech, 1988.

[6] G. M. Rebeiz, G.-L. Tan, and J. S. Hayden, "RF MEMS phase shifters: Design and applications," *IEEE Microw. Mag.*, vol. 3, pp. 72–81, 2002.

[7] R. D. Esman, M. J. Monsana, J. L. Dexter, and D. G. Cooper, "Microwave true time-delay modulator using fibre-optic dispersion," *Electron. Lett.*, vol. 28, no. 20, pp. 1905–1907, 1992.

[8] J. J. Lee *et al.*, "Photonic Wideband Array Antennas," *IEEE Trans. Antenna Propag.*, vol. 43, no. 9, 1995.

[9] J. L. Corral, J. Marti, S. Regidor, J. M. Foster, R. Laming, and M. J. Cole, "Continuously variable true time-delay optical feeder for phased-array antenna employing chirped fiber grating," *IEEE Trans. Microw. Theory Tech.*, vol. 45, no. 8, pp. 1531–1536, 1997.

[10] B. Vidal, D. Madrid, J. L. Corral, and J. Marti, "Novel photonic true-time-delay beamformer based on the free-spectral-range periodicity of arrayed waveguide gratings and fiber dispersion," *IEEE Photon. Technol. Lett.* , vol. 14, no. 1, pp. 1614–1616, 2002.

[11] M. A. Piqueras *et al.*, "Optically beamformed beam-switched adaptive antennas for fixed and mobile broad-band wireless access networks," *IEEE Trans. Microw. Theory Tech.*, vol. 54, no. 2, pp. 887–, 2006.

[12] N. A. Riza and S. Sumriddetchkajorn, "Micromechanics-based wavelength-sensitive photonic beam control architectures and applications," *Appl. Opt.*, vol. 39, no. 6, pp. 919–932, 2000.

[13] O. Raz, R. Rotman, and M. Tur, "Wavelength-controlled photonic true time delay for wide-band applications," *IEEE Photon. Technol. Lett.*, vol. 17, no. 5, pp. 1076–1078, 2005.

[14] O. Raz, S. Barzilay, R. Rotman, and M. Tur, "Fast switching and wide-band photonic beamformer with flat RF response and squintless scan performance," presented at the Proc. OFC 2007, OWU3, .

[15] R. J. Mailloux, "Operating modes and dynamic range of active space-fed arrays with digital beamforming," *IEEE Trans. Antenna Propag.*, vol. 54, no. 11, pp. 3347–, 2006.

[16] L. A. Coldren, G. A. Fish, Y. Akulova, J. S. Barton, L. Johansson, and C. W. Coldren, "Tunable semiconductor lasers: A tutorial," *J. Lightw. Technol.*, vol. 22, no. 1, pp. 193–202, 2004.

[17] M. C. Larson *et al.*, "High performance widely-tunable SG-DBR lasers," *Proc. SPIE*, vol. 4995, 2003, paper 13.

[18] C. H. Cox III, *Analog Optical Links*. Cambridge, U.K.: Cambridge Univ. Press, 2004.

[19] R. Rotman, O. Raz, and M. Tur, "Analysis of a true time delay photonic beamformer for transmission of a linear frequency-modulated waveform," *J. Lightw. Technol.*, vol. 23, pp. 4026–4036, 2005.

[20] J. C. Curlander and R. N. Mcdonough, *Synthetic Aperture RADAR - Systems and Signal Processing*. New York: Wiley, 1991, pp. 142–145.

[21] R. Rotman, O. Raz, S. Barzilay, S. Rotman, and M. Tur, "Wideband antenna patterns and impulse response of broadband RF phased arrays with RF and photonic beamforming," *IEEE Trans. Antennas Propag.*, vol. 55, no. 1, pp. 36–44, 2007.

[22] Industry sources, private communications.

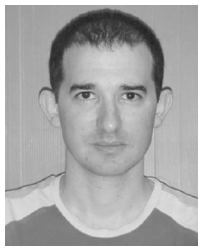

Oded Raz (S'05–M'07) was born in The Netherlands in 1970, and has been living in Israel since 1973. He received the B.Sc. degree in electrical engineering from the Technion-Israel Institute of Technology, Haifa, in 1993 and the M.Sc. and Ph.D. degrees from the Tel Aviv University, Tel Aviv, Israel, in 2002 and 2007, respectively.

He is currently a postdoctoral researcher with the Technical University of Eindhoven, The Netherlands, where he is working on high-speed optical transmission, integrated III-V optical circuits, and digital photonics. His other fields of interest include optical communications systems and integrated optical device in InP and SOI and optical buffering.

Ruth Rotman received the B.Sc. degree in electrical engineering and the M.Sc. degree from the Massachusetts Institute of Technology, Cambridge, in 1983 and 1985, respectively. He received the Ph.D. degree from Tel Aviv University, Tel Aviv, Israel, in 2008 in the area of microwave photonics.

Sharon Barzilay received the B.Sc. degree from the Technion-Israel Institute of Technology, Haifa, in 2004 and the M.Sc. degree from Tel Aviv University, Tel Aviv, Israel, in 2006, both in electrical engineering.

She is currently with Elta Electronics Industries, Tel Aviv, where her interests include photonic beamforming, Elint and Commint Systems.

Moshe Tur (M'87–SM'94–F'98) received the B.Sc. degree in mathematics and physics from the Hebrew University, Jerusalem, Israel, in 1969, the M.Sc. degree in applied physics from the Weizmann Institute of Science, Rehovot, Israel, in 1973, and the Ph.D. degree from Tel-Aviv University, Tel-Aviv, Israel, in 1981.

He is presently the Gordon Professor of Electrical Engineering at the School of Electrical Engineering, Tel-Aviv University, where he has established a Fiber-Optic Sensing and Communication Laboratory. He authored or coauthored more than 250 journal and conference technical papers with emphasis on fiber-optic sensing, polarization mode dispersion, microwave photonics, and advanced fiber-optic communication systems.

Dr. Tur is a Fellow of both the IEEE and the Optical Society of America and a Member of SPIE.